Bioactive Materials 36 (2024) 541–550

Contents lists available at ScienceDirect

Bioactive Materials

journal homepage: www.keaipublishing.com/en/journals/bioactive-materials

In situ sustained release hydrogel system delivering GLUT1 inhibitor and chemo-drug for cancer post-surgical treatment

Lanqing Wang [a], Zi Mei [b], Guanyu Jin [b], Hao Liu [b], Shixian Lv [b], Runjia Fu [c,**], Muxing Li [b,***], Cuiping Yao [a,*]

[a] Institute of Biomedical Photonics and Sensing, School of Life Science and Technology, Key Laboratory of Biomedical Information Engineering of Ministry of Education, Xi'an Jiaotong University, Xi'an, 710049, China
[b] School of Stomatology, School of Materials Science and Engineering, Department of General Surgery, Third Hospital, Peking University, Beijing, 100871, China
[c] Department of Oncology, The Second Hospital, Cheeloo College of Medicine, Shandong University, Jinan, 250033, China

ARTICLE INFO

Keywords:
Chitosan-based hydrogel
Drug delivery
Controlled-release
Abscopal effect
Polymer carriers

ABSTRACT

Systematic administration of small molecular drugs often suffered from the low efficacy and systemic toxicity in cancer therapy. In addition, application of single mode drug usually leads to unsatisfactory therapeutic outcomes. Currently, developing multimodal-drug combination strategy that acts on different pathways without increasing side effects remains great challenge. Here, we developed a hydrogel system that co-delivered glycolysis inhibitor apigenin and chemo-drug gemcitabine to realize combination strategy for combating cancer with minimal systemic toxicity. We demonstrated that this system can not only eliminate tumor cells *in situ*, but also induce abscopal effect on various tumor models. These results showed that our study provided a safe and effective strategy for clinical cancer treatment.

1. Introduction

Cancer is one of the leading causes of death worldwide, with approximately 20 million people diagnosed with cancer each year. Breast cancer, lung cancer, liver cancer, colon cancer, and prostate cancer are the most common types of cancer [1–5]. Surgery combined with chemotherapy is still the primary method for treating cancers. The clinical results of using chemo-drugs for the treatment of cancer demonstrated that monotherapy often led to the development of drug resistance [6]. Combination therapy has highlighted the potential for long-term cancer growth control and sustained response by targeting different pathways and remodeling tumor microenvironment [7]. That also poses challenges such as timing coordination and enhanced side effects [8–10]. By targeting tumor cell-specific metabolic pathways, it is possible to selectively eliminated tumor-associated cells while minimizing the side effects to normal healthy cells. Therefore, tremendous efforts have been focused on discovery of potent agents that target tumor metabolic pathways (see Scheme 1).

In 1924, Otto Warburg discovered that tumor cells tend to convert glucose into lactate through glycolysis [11–14], even in the presence of sufficient oxygen for mitochondrial oxidative phosphorylation [15,16]. Of notable interest is glucose transporter 1 (GLUT1), an extensively distributed glucose transporter which is highly expressed in almost all tumor cells, increase intracellular glucose uptake for glycolysis [17]. Therefore, reducing the degree of tumor glycolysis by decreasing GLUT1 and thus reducing the energy source of tumor cells is a crucial strategy. Some preclinical studies have indicated that glycolysis inhibitors exhibit notable targeting specificity and have the potential to serve as adjunctive therapies to existing standard chemotherapy [18–21]. Besides, several glycolysis inhibitors have shown the ability to remodel the tumor immune-suppressive microenvironment, which holds great potential for effective cancer post-surgical treatment. Nevertheless, the efficacy of GLUT1 inhibitors as anticancer drugs is still limited, and the side effects are still undesirable, indicating delivery and combination strategies are needed for practical use of GLUT1 inhibitors [22].

Several bioactive molecules derived from natural plant ingredients

Peer review under responsibility of KeAi Communications Co., Ltd.
* Corresponding author.
** Corresponding author.
*** Corresponding author.
E-mail addresses: furunjia@pku.edu.cn (R. Fu), limuxing@hsc.pku.edu.cn (M. Li), zsycp@xjtu.edu.cn (C. Yao).

https://doi.org/10.1016/j.bioactmat.2024.06.034
Received 9 May 2024; Received in revised form 10 June 2024; Accepted 25 June 2024

are thought to have potential in treating cancers through inhibition of GLUT1 [23–25]. For instance, apigenin (4′,5,7-trihydroxyflavone) was selected as GLUT1 inhibitor for its glycosylated modification [26], anti-tumor effects [27], low toxicity [28] and immunoenhancement [29]. The most important aspect is that apigenin has minimal toxicity to normal cells. In addition, apigenin is inexpensive and easily accessible. Studies have been focused on *in vitro* chemo-sensitization and reduced nephrotoxicity i*n vivo*, or on *in vitro* synergistic antiproliferative effects, or on molecular mechanisms of action of apigenin in combination with chemotherapy agents [30]. However, apigenin has low bioavailability, making it challenging to achieve the desired effects, which requires delivery strategies of apigenin to enhance its anti-tumor activity. Up to now, several drug carriers delivering apigenin as GLUT1 inhibitor for cancer treatment had been reported, however, these delivery systems only received moderated antitumor effect, indicating inhibition of GLUT1 may not be sufficient enough towards effective cancer treatment [31]. Combination of apigenin with chemo-drugs such as 5-fluorouracil has been proved to be more effective, but also led to increased side effects. Therefore, there is an urgent need to develop delivery strategy for combination of apigenin and chemo-drugs with high efficiency and low side effects.

Compared to systemic administration, local drug delivery *via in situ* release offers the advantage of gradual drug release within the body, thereby extending the duration of drug exposure and reducing the required dosage, resulting in enhanced therapeutic efficacy and increased safety [32–34]. For example, hydrogels can slowly release drugs in the body for several days, which greatly extend the time of drug action, reduce drug dosage and toxic side effects, and significantly improve the effectiveness of drug treatment [35,36]. Additionally, lots of synthetic or natural polymers can be readily used in hydrogel fabrication. For instance, the cost-effective polysaccharide-based natural polymers (*e.g.,* chitosan, dextran and hyaluronic acid) with high biocompatibility, excellent *in vivo* safety profiles, simplified hydrogel formulation and preparation have been extensively used in various hydrogel systems [37]. Therefore, we proposed that the co-delivery of apigenin as a glycolysis inhibitor with gemcitabine within a polysaccharide-based *in situ* hydrogel system may address the issues of GLUT1 inhibitors and provide more effective and safe treatment towards post-surgical cancer treatment [38–40].

Herein, we first reported a hydrogel drug delivery system to co-deliver apigenin and gemcitabine for post-surgical cancer treatment of colorectal cancer. The hydrogel used in this work was prepared from oxidized sodium alginate and carboxymethyl chitosan through Schiff-base reaction. To test the abscopal effect, the recurrence model and re-injection model were utilized in this study. Results showed that the designed strategy achieved excellent anti-tumor effects for different tumor models. In addition, the tumor immune-suppressive microenvironment was greatly changed during the treatment. This approach offered great advantages towards safe and effective post-surgical treatment. These findings in our study will provide a foundation for further exploration of glycolysis inhibitors for cancer therapy.

2. Result and discussion

2.1. Fabrication and characterization of the chitosan-based hydrogel

The hydrogel preparation method involved the oxidation of sodium alginate to form oxidized sodium alginate, followed by a Schiff-base reaction between the aldehyde groups of oxidized sodium alginate and the amino groups of carboxymethyl chitosan, and finally crosslinking to prepare chitosan-based hydrogels. The schematic diagram of this synthesis method was illustrated (Fig. 1A). After screening the properties of hydrogels according (Table S1), carboxymethyl chitosan with 4 % concentration and sodium alginate oxide with 10 % concentration were selected to form hydrogel to complete the follow-up experiment.

The structure of sodium alginate was analyzed by fourier transform infrared spectroscopy (FTIR), and the characteristic absorption peak in the range of 1700 cm^{-1} to 1750 cm^{-1} corresponded to the C═O double bond of the aldehyde group was observed [41] (Fig. S1). Additionally, hydrogen nuclear magnetic resonance spectroscopy (^{1}H NMR) confirmed the successful oxidation of sodium alginate and the presence of cross-linking sites in the hydrogel [42] (Fig. S2).

Subsequently, ultraviolet absorption measurements were utilized to investigated the drug release from the hydrogel (Fig. 1B). The hydrogel reached 95 % of the maximum drug release after the tenth day, indicated that the hydrogel has a sustained drug release performance.

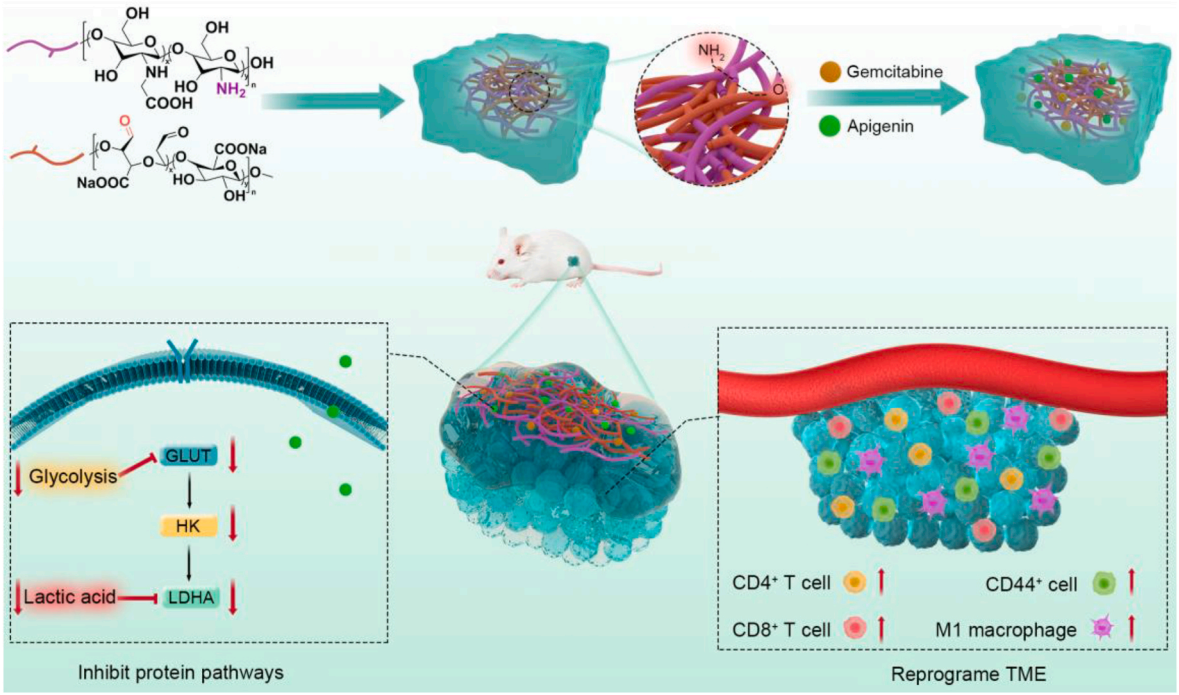

Scheme 1. *In situ* sustained release hydrogel system involved GLUT1 inhibitor and chemo-drug to improve anti-tumor efficacy.

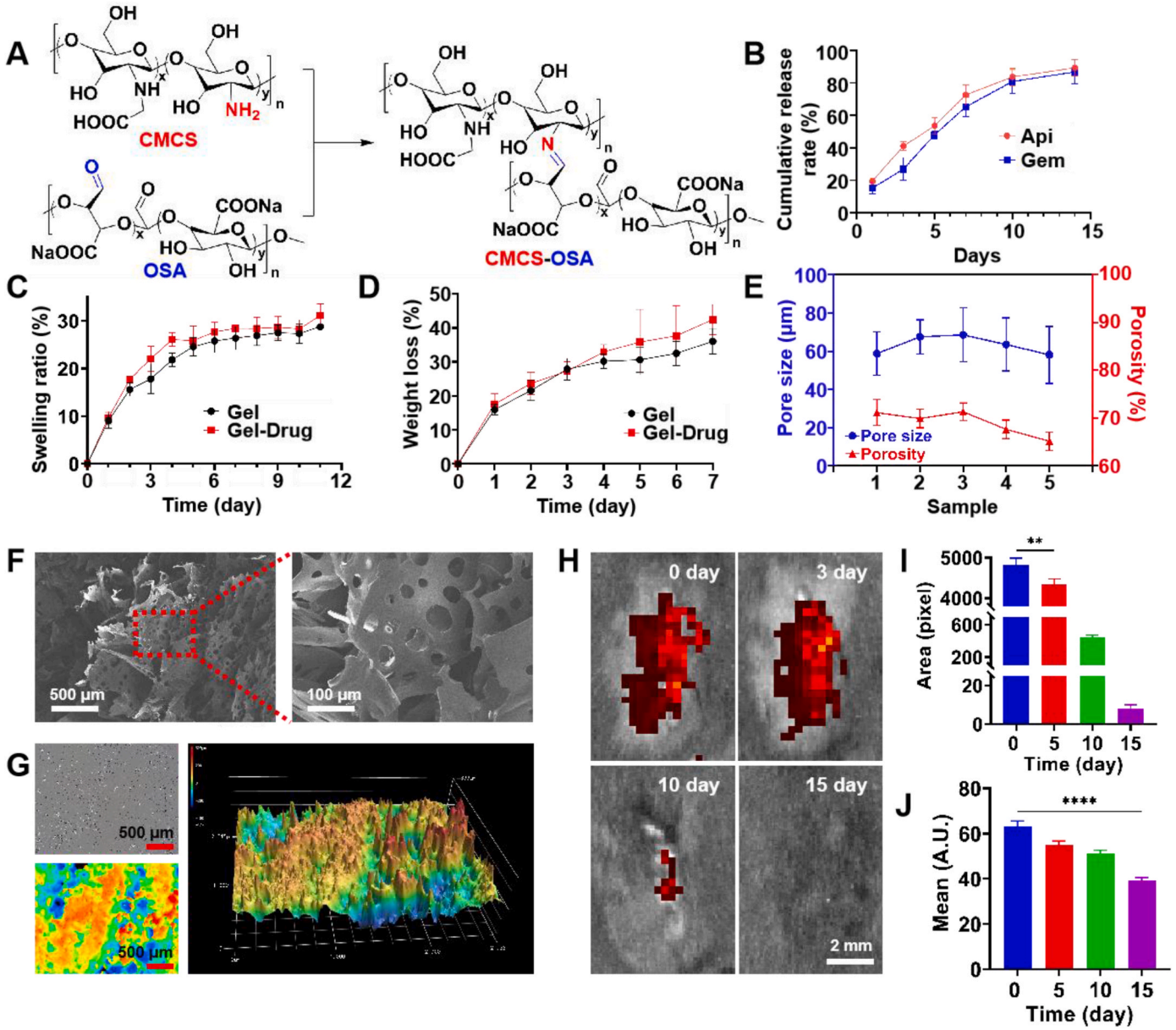

Fig. 1. Synthesis and characterization of chitosan-based hydrogel. A) Synthesis of hydrogel. B) Release rate of hydrogel loaded with Api or Gem in PBS solution (n = 3). C) Swelling Ratio of the hydrogel over 4 days (n = 3). D) Weight loss rate of the hydrogel over 7 days (n = 3). E) Quantitative analysis of pore size and porosity of the hydrogel (n = 3). F) Scanning electron microscopy image of the internal microstructure of the hydrogel. G) Optical scanning image of the surface microstructure of the hydrogel (2.8 * 2.1 * 0.9 μm). H) *In vivo* degradation fluorescence imaging of the hydrogel in mouse (0, 3, 10, 15 days). I) Quantitative analysis of the fluorescent range in the degradation images of the hydrogel *in vivo* (n = 3). J) Quantitative analysis of the fluorescent intensity in the degradation images of the hydrogel *in vivo* (n = 3). *, $P < 0.05$, **, $P < 0.01$, ***, $P < 0.001$ and ****, $P < 0.0001$.

Furthermore, the swelling behavior of hydrogels can ensure drug exchange and release *in vivo*. Therefore, the swelling ratio (Fig. 1C) and erosion rate (Fig. 1D) of the hydrogel were measured in phosphate buffered saline (PBS, pH = 7.4). Once the aqueous solution entered the hydrogel, the polymer chains interacted with the solution due to osmotic pressure, resulting in gel stretching and swelling. There were no significant differences in the swelling and erosion rates between the drug-loaded hydrogel and the base hydrogel. The swelling ratio stabilized after the day 3. Once the osmotic pressure reached equilibrium, the gel stretch was constrained, leading to gel degradation. At this point, the erosion rate exhibited a slow increase, and the total erosion reached 38 % by the fifth day before gradually stabilizing.

To further validate the formation of chitosan-based hydrogels, compression test was conducted using a universal testing machine. The results revealed no significant differences in the mechanical properties between the drug-loaded hydrogel and the base hydrogel. Both hydrogels exhibited the ability to resist compression (Fig. S3). This suggested that the hydrogels can be utilized in various *in vivo* and *in vitro* experiments, as well as surgical procedures at tumor sites.

The structure of the hydrogel network plays a critical role in drug release and gel degradation rates. Scanning electron microscopy (SEM) was employed to observe the internal microstructure of the hydrogel (Fig. 1F). The SEM images demonstrated a complex porous and interconnected structure within the freeze-dried hydrogel material, with relatively uniform pore sizes. Pore sizes ranging from 60 to 90 μm were measured at five randomly selected locations (Fig. 1E). The porosity, determined using the Archimedes method, was found to be 60 %–70 %. These results indicated that the hydrogel was suitable for physiological

information exchange and possessed a certain level of mechanical strength. Additionally, an optical scanning imaging device to observe the surface microstructure of the scaffold material and measure the roughness at the detection site, which was 595 μm (−200 μm–395 μm) (Fig. 1G). This verified that the rough surface morphology of the material facilitates cell recruitment, enhances cell adhesion, promotes cell activity, and thus improves the recruitment of T cells and the efficacy of the drug against tumor cells.

The *in vivo* degradation of the hydrogel significantly affects the efficacy of combination therapy. The volume changes of the hydrogel during the treatment were observed, and the fluorescent area and intensity were quantitatively analyzed (Fig. 1H–J). The results revealed a

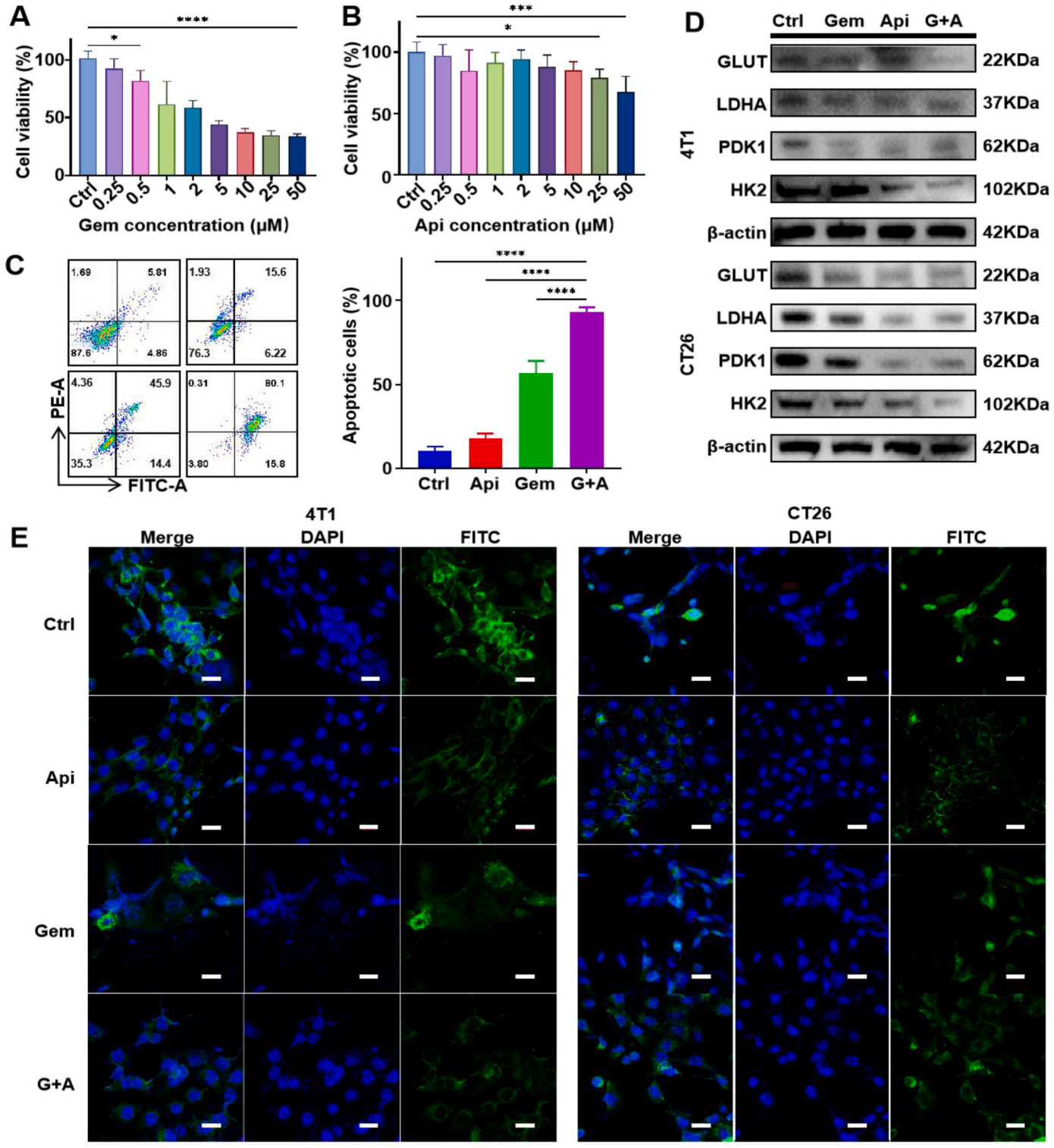

Fig. 2. Synergistic effects of apigenin and gemcitabine on tumor cells. A-B) Optimal concentration selection of apigenin and gemcitabine in cancer cells (CT26) using the CCK-8 assay (n = 3). C) Detection and quantitative analysis of the pro-apoptotic effect on cancer cells (CT26) staining (n = 3). D) Analysis of glycolysis pathway targets in tumor cells (CT26, 4T1) treated with different drug combinations using western blot. E) Immunofluorescent staining of GLUT1 in tumor cells (CT26, 4T1) treated with different drug formulations (scale bar: 100 μm). *, $P < 0.05$, **, $P < 0.01$, ***, $P < 0.001$ and ****, $P < 0.0001$.

gradual degradation process of the hydrogel, allowing for the gradual release of drugs and maintaining a sustained drug concentration during the treatment. As the degradation of the hydrogel increased, the drug release rate also increased, enabling a gradually increasing drug delivery rate and improving the efficiency of the treatment outcome.

2.2. Cytotoxicity in vitro

CCK-8 cell experiments were conducted to optimize the concentrations of two drugs, apigenin (Api) and gemcitabine (Gem), and evaluate their inhibitory effect on tumor cell proliferation. A range of concentrations (0.25/0.50/1.0/2.0/5.0/10/25/50 μM) was selected based on preliminary experiments and literature reports [43,44]. The selected concentrations were applied to CT26 cell lines. The results of the concentration screening experiments for apigenin and gemcitabine (Fig. 2A and B) indicated that apigenin had a minimal inhibitory effect on cell proliferation, while a significant inhibitory effect was observed when the two drugs were used in combination (Fig. S4). Gemcitabine exhibited a dose-dependent inhibition on cell proliferation within a certain concentration range. Calculation of IC_{50} further indicated a synergistic effect between apigenin and gemcitabine within a specific concentration range. The same drug concentrations were also applied in 4T1 mouse breast cancer cells and B16F10 mouse melanoma cells (Figs. S5–S6). Based on Jin's Formula, concentrations of 1.0 μM apigenin

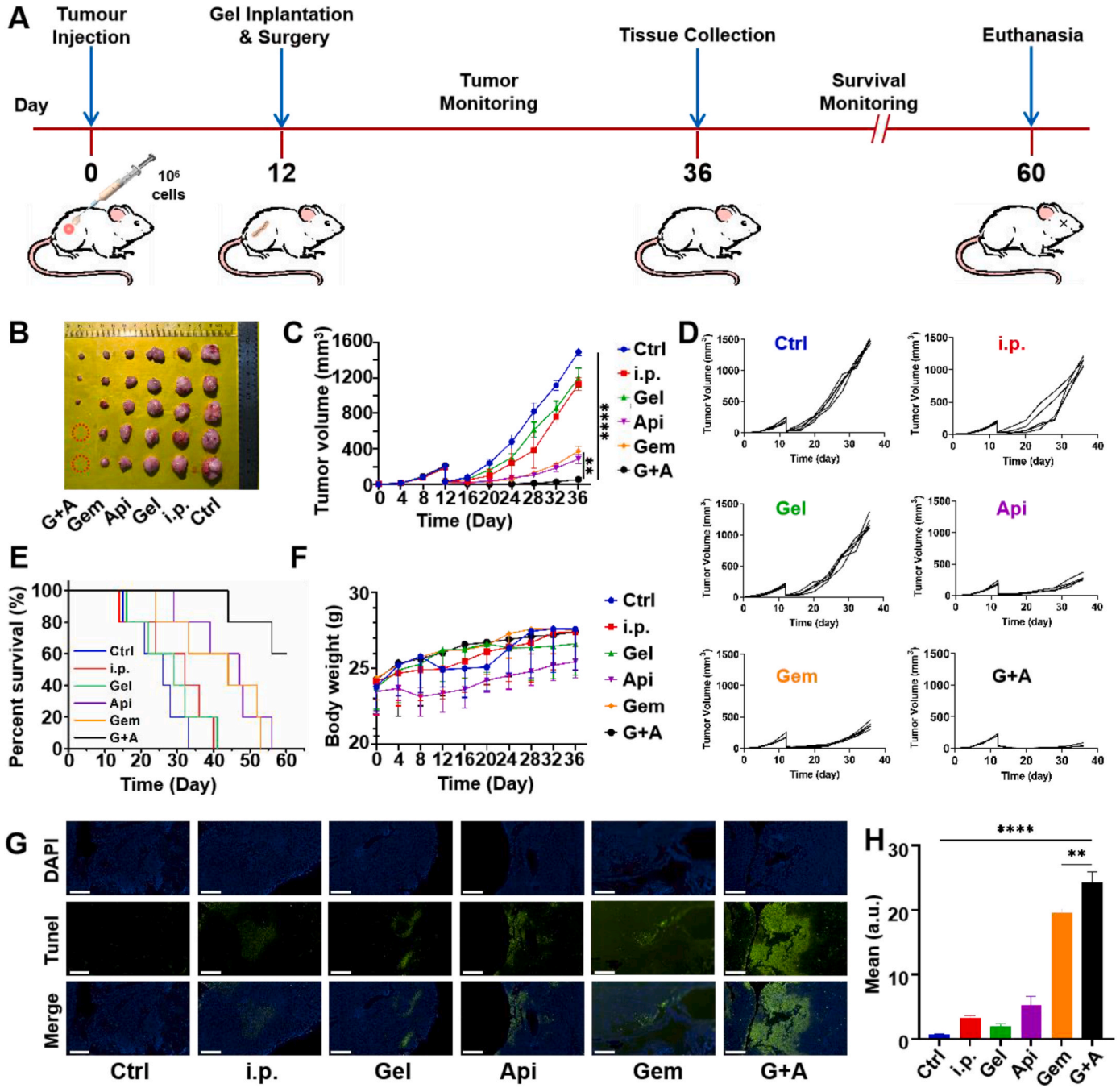

Fig. 3. Therapeutic effect of combination drugs on cancer recurrence model. A) Tumor cell injection in the CT26 recurrence model. B) Imaging of solid tumors. (Scale bar as shown in the figure).C-D) Tumor volume changes in each group. (n = 5). E) Survival period presentation of mice in each group. (n = 5). F) Body weight changes in each group. (n = 5). G-H) TUNEL staining levels in tumor and the quantitative analysis. (TUNEL staining shown in green, n = 3, scale bar: 500 μm). *, $P < 0.05$, **, $P < 0.01$, ***, $P < 0.001$ and ****, $P < 0.0001$.

and 1.0 μM gemcitabine were selected for subsequent experiments.

$$Q = E_{a+b} / (E_a + E_b - E_a * E_b) = 68\% / (38\% + 11\% - 4.18\%) \approx 1.52 > 1.15$$

The effect of combination therapy on cell apoptosis was investigated in order to optimize the drug use for further studies. A cell apoptosis assay was conducted to analyze the effects of combining apigenin and gemcitabine on tumor cell apoptosis. The results demonstrated that in the control group, the average percentage of apoptotic cells was 14.2 ± 1.1 % (Fig. 2C). When used alone, the inhibitory effect of Api drug on tumor cells was not significant. Gem had an obvious inhibitory effect on tumor cells, with an apoptosis rate of 58.2 ± 6.0 %. In contrast, the combination therapy group (G + A) exhibited an average percentage of apoptotic cells of 94.1 ± 1.8 %, indicating a significant increase in apoptotic cells compared with the other groups. The results of the cell apoptosis assay validated the excellent effectiveness of combination therapy in inducing cell apoptosis.

Western blotting was used to evaluate the mechanism through target protein expression and activation. Changes in glycolysis such as Glut, LDHA, PDK1, HK2 were measured and analyzed (Fig. 2D). The cells were divided into four groups: Control (Ctrl), apigenin (Api), gemcitabine (Gem), and gemcitabine & apigenin (G + A). CT26 and 4T1 tumor cells were used in this assay. The results showed that in the group without the use of glycolysis inhibitors, protein bands in various pathways had significant staining. Among these, the protein bands in the G + A group had the weakest staining, indicating that apigenin was an effective inhibitor of the glycolysis pathway. Furthermore, when co-administered with gemcitabine, apigenin further enhanced the glycolysis inhibitory effect.

To investigate the impact of combination therapy on protein migration, an immunofluorescence experiment was conducted using CT26 and 4T1 tumor cells (Fig. 2E). The intensity and localization of the fluorescent signals in the different cell groups were then observed and compared. The results of the experiment displayed a significant inhibitory effect on GLUT1 protein migration in the group treated with Api, with the majority of the target protein fluorescence.

2.3. Antitumor evaluation on recurrence model in vivo

The anti-tumor effect of hydrogel was first studied in the CT26 mouse cancer model (Fig. 3A). After 12 days of inoculation, when the tumor volume reached the desired range (150–200 mm^3), the mice were randomly divided into six groups: Ctrl, Api, Gem, G + A and intraperitoneal injection (i.p.), hydrogel (Gel), and subjected to tumor resection surgery. After anesthesia, approximately 10 % v/v of the tumor mass was retained. Subsequently, hydrogels loaded with different drugs were implanted into the resected tumor sites. To minimize the impact on the mice, the surgical procedure was limited to approximately 10 min per animal.

On day 36 after injection, 5 mice from each group were euthanized, and residual tumors were collected for histological analysis (Fig. 3B). The data indicated that the tumor volume in the G + A group was relatively smaller, suggesting that the treatment regimen of the G + A group had a positive therapeutic effect and inhibited tumor growth. The tumor volume of mice in different groups was measured using a caliper, and the results for each group were presented separately (Fig. 3C and D). The results demonstrated a significant inhibitory effect on tumor growth during the treatment period in the G + A group.

Furthermore, the survival time of the remaining mice were recorded until day 60 after tumor injection. According to the experimental results (Fig. 3E), the mice in the G + A group maintained a 60 % survival rate after 60 days post-injection, exhibiting a much longer survival time compared to the control groups. The mice in the Api and Gem groups experienced death between days 53–56 post-injection, while those in the i.p. and Gel groups experienced death around 40 days post-injection. This suggested that the treatment of G + A group can effectively prolong the survival period and survival rate of tumor bearing mice.

The body weight of the remaining mice was also recorded and observed them during the treatment period (Fig. 3F). According to the data, there was no significant change in the recovery of body weight among the mice in the G + A group compared to the other groups. All groups showed a slow and gradual increase in body weight. This suggested that the treatment regimen of G + A group did not have detectable side effects.

Terminal Deoxynucleotidyl Transferase mediated dUTP Nick-End Labeling (TUNEL) staining experiment was conducted to detect DNA fragmentation within the tumor cells in the tissue sections, serving as an indicator of cell apoptosis level (Fig. 3G). The results demonstrated that the number of TUNEL-positive cells (indicating DNA fragmentation) in the G + A group was significantly higher than that in the other groups, which was further supported by the quantitative analysis of fluorescence intensity (Fig. 3H). The high apoptosis rate in G + A group suggested that this treatment displayed a positive role in inhibiting tumor growth and promoting cell apoptosis.

By observing and comparing the hematoxylin-eosinstaining (H&E) staining results of tumors in different groups of mice, the antitumor effects of different treatments were further evaluated. According to the results (Fig. 4A), cells in the G + A group exhibited abnormal tissue structure, changes in nuclear and cytoplasmic morphology, as well as noticeable infiltration of inflammatory cells. In summary, combined treatment with G + A demonstrated significant effectiveness in promoting tumor necrosis and inhibiting tumor growth, when compared to the monotherapy of Api and Gem. The results of H&E staining on the animal organ sections showed no significant pathological changes in the organs (Fig. S7), which indicated that the combination of the two drugs did not cause detectable damage to the mice.

Tumor-associated macrophages (TAMs) were the most common immune cells in the tumor microenvironment. In this study, specific markers F4/80 and CD86 were used to identify and analyze the M1 phenotype of macrophages (Fig. 4B). The results showed a high proportion of macrophages expressing the dual-positive phenotype of F4/80 and CD86 in the G + A group, followed by a higher expression proportion in the Api group compared to the other three groups. Quantitative analysis indicated that the G + A group had a higher percentage and intensity level of macrophages expressing F4/80 and CD86 (Fig. 4C–S9), indicating a higher content of M1 macrophages in the G + A group and a highly polarized state. Based on these results, the activation and regulation of M1 macrophages were assessed by the treatment method used in this study and further investigate their functions and mechanisms.

The CD8/CD3 T cell ratio within the tumor is an important indicator for evaluating tumor immune cell infiltration and activity. The T cell ratio within the tumor tissue of different groups was analyzed using flow cytometry (Fig. 4D), and the results were quantitatively and localization analysis (Fig. 4E–F, S8). It was observed that the CD8/CD3 T cell ratio in the G + A group was significantly higher compared to the other groups. This indicated a higher proportion of $CD8^+$ T cells relative to the total T cell population within the tumor tissue of the G+A group, and suggested the presence of a robust cellular immune response in the tumor immune environment of the G + A group, where $CD8^+$ T cells played a vital role in anti-tumor immunity.

The results together indicated that the treatment of hydrogel loaded with G + A exhibited potent antitumor effects with minimal side effects. Characterization of the tumor interior revealed that the G + A group not only exhibited a favorable anti-tumor recurrence effect but also exerted the ability to remodel tumor immune suppressive environment. These findings suggested that this treatment regimen may serve as an effective therapeutic strategy with potential clinical application.

2.4. Antitumor evaluation on metastasis tumor model in vivo

To further validate the anti-tumor effect of the drug-loaded hydrogel,

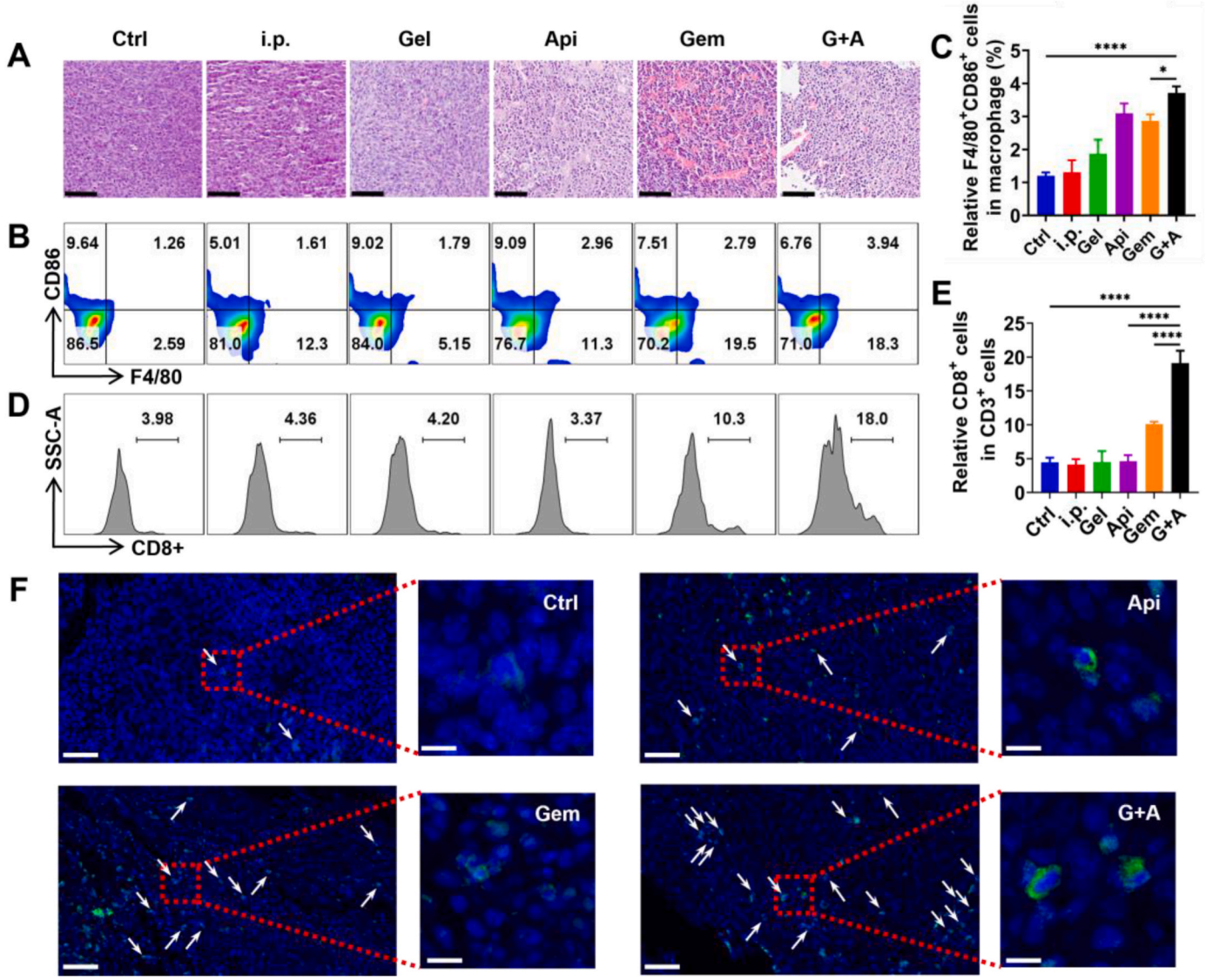

Fig. 4. Therapeutic effects of combination drugs on cancer recurrence model: H&E staining, flow cytometry, and CD8 staining. A) H&E staining of tumor sections in each group. (scale bar: 100 μm) B) Proportions of M1 macrophages in tumor tissues of each group. C) Quantitative analysis of M1 macrophages in tumor tissues of each group (n = 5). D) Proportions of $CD8^+/CD3^+$ cells in tumor tissues of each group. E) Quantitative analysis of $CD8^+/CD3^+$ cells in tumor tissues of each group (n = 5). F) CD8 staining in tumor tissues of each group (Ctrl, Api, Gem, G + A) (CD8 staining shown in green, scale bar: 50 μm, 10 μm). *, $P < 0.05$, **, $P < 0.01$, ***, $P < 0.001$ and ****, $P < 0.0001$.

a mouse metastasis tumor model experiment was conducted. According to previous results, combined treatment group had the best treatment effect, in metastasis model, the combined group was used as the experimental group and the untreated group as the control group. Subsequently, the tumor tissues were monitored, and on the 36th day after injection, five mice from each group were euthanized (Fig. 5A).

Firstly, statistical analysis on the changes in body weight of the mouse groups were conducted (Fig. 5B). The data showed a gradual and almost negligible difference in weight gain between the two groups, demonstrating that the combined use of G + A in the metastasis model did not adversely affect the health of the mice. Secondly, the changes in primary tumors and metastatic lesions were statistically analyzed in the two groups (Fig. 5C–E). Tumor volume in the control group increased rapidly post-surgery, while the G + A group exhibited minimal changes in tumor volume. Additionally, in the analysis of metastatic lesions, it was observed that the G + A group still exerted a significant inhibitory effect on the growth of metastatic lesions. By the 24th day post-surgery, most of the metastatic lesions in the G + A group did not exceed 100 mm^3, while the control group showed a slow initial growth followed by rapid expansion. In conclusion, the treatment of G + A group demonstrated effective therapeutic and inhibitory effects on tumor metastasis.

In the metastasis model, the ratios of $CD4^+/CD3^+$ and $CD8^+/CD3^+$ T cells were important indicators for evaluating the distribution of tumor immune cell types and the immune environment. Flow cytometry analysis and quantitative analysis were performed (Fig. 5F and G). The results indicated that the $CD4^+/CD3^+$ ratio was higher in the G+A group compared to the Ctrl group, including an increased abundance of $CD4^+$ T lymphocytes relative to the total T lymphocytes in the tumor tissue of the G+A group. Similarly, the $CD8^+/CD3^+$ ratio was higher in the G+A group compared to the Ctrl group, indicating an elevated ratio of $CD8^+$ T lymphocytes relative to the total T lymphocytes in the tumor tissue, which was beneficial to prevent tumor metastasis and recurrence.

2.5. Antitumor evaluation on re-challenge model in vivo

The anti-tumor effect of the designed drug-loaded hydrogel was finally validated in the mouse re-challenge mode. (Fig. 6A). First, statistical analysis of the differences in weight gain among the groups of

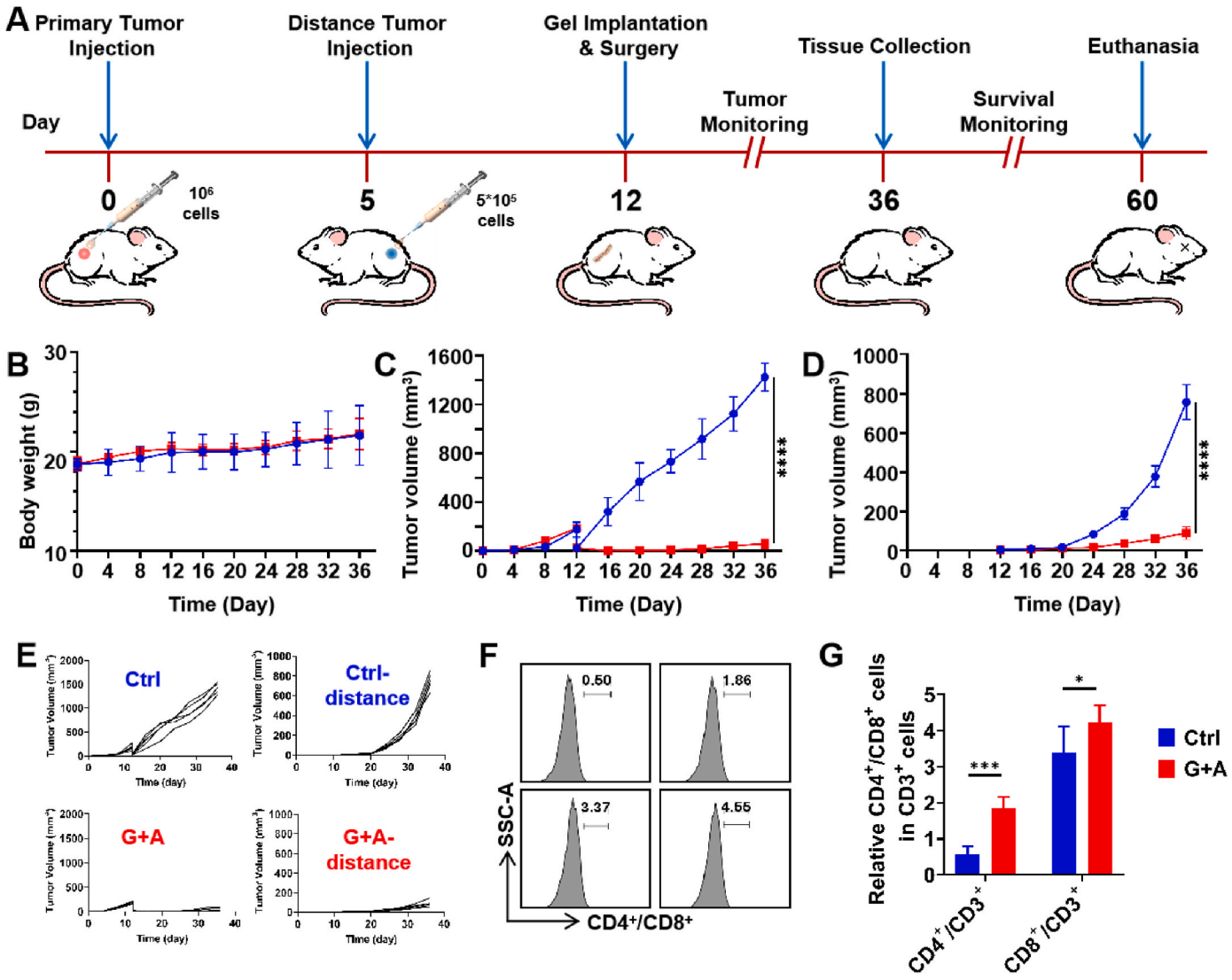

Fig. 5. Therapeutic effects of combination therapy on cancer metastasis model. A) Treatment schedule for CT26 metastasis model. B) Body weight changes in each group (n = 5). C) Initial tumor volume changes in each group (n = 5). D) Metastases volume changes in each group (n = 5). E) The initial tumors and metastases volume changes in each group. F-G) Flow cytometric analysis and quantification of $CD4^+/CD3^+$ and $CD4^+/CD8^+$ cells in tumor tissues in each group (Ctrl, Api, Gem, G + A) (n = 5). *, $P < 0.05$, **, $P < 0.01$, ***, $P < 0.001$ and ****, $P < 0.0001$.

mice showed no significant change in weight gain between the two groups (Fig. 6B), indicating that the combined use of G + A in the re-challenge model had no adverse effect on the overall health of the mice. Then, the volume changes of the regenerated tumors were analyzed (Fig. 6C and D). The tumor volume of the Ctrl group increased after reinjection, while the tumor volume of G + A group increased much slower. The results showed that group G + A had a significant inhibitory effect on the growth of regenerated tumors.

Flow cytometry analysis and quantitative analysis were performed for the $CD8^+$ ratio (Fig. 6E and F). The results revealed that the $CD8^+/CD3^+$ ratio was higher in the G+A group compared to the Ctrl group. This indicated an increase of $CD8^+$ T lymphocytes in the tumor tissue of the G+A group, revealing enhanced immune response against the tumor during the treatment.

The population of $CD44^+$ $CD62L^+$ cells was analyzed to evaluate the activation of memory T cells in tumor immune response. Based on the results (Fig. 6G and H), the proportion of $CD44^+$ $CD62L^+$ cells were detected the immune memory effect ($CD44^+$ $CD62L^+$: Tcm, $CD44^+$ $CD62L^-$: Tem). In G + A group, higher Tcm and lower Tem ratio were observed when compared with control group. These findings suggested an increase in immune memory T cells, enhanced immune protection and memory for the designed treatment group.

In summary, the results in the mouse re-challenge model had confirmed that the combination therapy of G + A effectively enhanced tumor prognosis, increased the suppressive capacity against tumor recurrence, and reduced the likelihood of tumor recurrence. This treatment approach was effective and safe.

3. Conclusion

In summary, our study demonstrated that the combination of apigenin and gemcitabine in the chitosan-based hydrogel was an effective and safe treatment for cancer post-surgical treatment. The therapeutic approach of delivering the GLUT1 inhibitor and chemo-drug using the hydrogel showed excellent tumor inhibition activity *in vivo* against different tumor models with minimal side effects. Due to the remodeling of tumor immunosuppressive microenvironment by targeting tumor metabolic pathways, such strategy holds great potential for clinical cancer therapy through significant inhibition of tumor metastasis and recurrence. Detailed studies are needed to further validate the safety and efficacy for clinical translation.

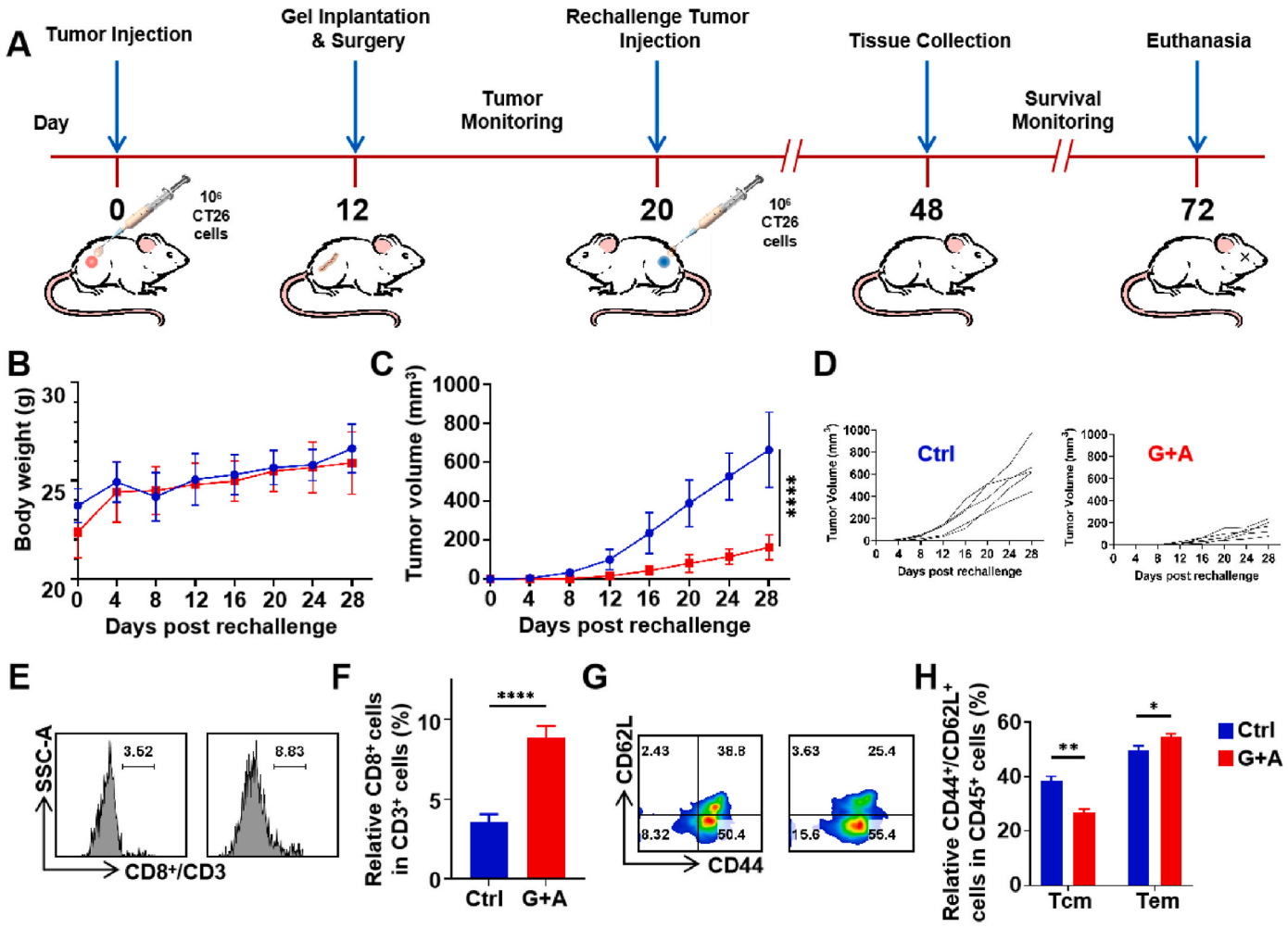

Fig. 6. Therapeutic effects of combination therapy on cancer re-injection model. A) Treatment schedule for CT26 re-injection model. B) Body weight changes in each group after re-injection (n = 5). C) The second tumors volume changes in each group after re-injection (n = 5). D) Individual primary tumor and secondary tumor volume changes in each group after reinjection. E-F) Flow cytometric analysis and quantification of $CD8^+/CD3^+$ cells in tumor tissues in each group (n = 5). G-H) Flow cytometric analysis and quantification of $CD44^+/CD62L^+$ and $CD44^+/CD62L^-$ cells in tumor tissues in each group (n = 5). *, $P < 0.05$, **, $P < 0.01$, ***, $P < 0.001$ and ****, $P < 0.0001$.

Experimental section

The experimental details are provided in the Supporting Information.

Ethics approval and consent to participate

1.The animal experiment program is reasonably designed, and the experimental operation meets the requirements of ethical review;
2.The number of experimental animals is set reasonably, and the experimental cycle is in line with their physiological characteristics;
3.The project involves operations that cause harm to animals, all of which have appropriate treatment measures;
4.The project has taken appropriate euthanasia measures for the animals after the experiment.

CRediT authorship contribution statement

Lanqing Wang: Writing – original draft, Data curation, Conceptualization. **Zi Mei:** Software, Project administration. **Guanyu Jin:** Formal analysis. **Hao Liu:** Resources. **Shixian Lv:** Software, Investigation. **Runjia Fu:** Supervision. **Muxing Li:** Validation. **Cuiping Yao:** Writing – review & editing, Funding acquisition.

Declaration of competing interest

The authors declare no conflicts of interest.

Acknowledgments

This work was supported by the National Natural Science Foundation of China (62175198, 52273114, 82103323, 82003992, and U22A2092), the Fundamental Research Funds for the Central Universities (xtr062022002), Key Research and Development Program of Shaanxi Province under Grant No. 2022ZDLSF04-09, and Beijing Natural Science Foundation (7222214).

Appendix A. Supplementary data

Supplementary data to this article can be found online at https://doi.org/10.1016/j.bioactmat.2024.06.034.

References

[1] R.L. Siegel, K.D. Miller, N.S. Wagle, A. Jemal, Cancer statistics, Ca-Cancer J. Clin. 73 (2023) (2023) 17–48.
[2] Y.C. Wu, S.X. Yang, J.Q. Ma, Z.C. Chen, G.H. Song, D.N. Rao, Y.F. Cheng, S. Y. Huang, Y.F. Liu, S. Jiang, J.X. Liu, X.W. Huang, X.Y. Wang, S.J. Qiu, J.M. Xu, R. B. Xi, F. Bai, J. Zhou, J. Fan, X.M. Zhang, Q. Gao, Spatiotemporal immune

landscape of colorectal cancer liver metastasis at single-cell level, Cancer Discov. 12 (2022) 134–153.
[3] J.J. Huang, D.I.I.I. Lucero-Prisno, L. Zhang, W.H. Xu, S.H. Wong, S.C. Ng, M.C. S. Wong, Updated epidemiology of gastrointestinal cancers in East Asia, Nat. Rev. Gastroenterol. Hepatol. 20 (2023) 271–287.
[4] R. Kalluri, K.M. McAndrews, Review the role of extracellular vesicles in cancer, Cell 186 (2023) 1610–1626.
[5] H. Rumgay, M. Arnold, J. Ferlay, O. Lesi, C.J. Cabasag, J. Vignat, M. Laversanne, K. A. McGlynn, I. Soerjomataram, Global burden of primary liver cancer in 2020 and predictions to 2040, J. Hepatol. 77 (2022) 1598–1606.
[6] L.S. Goodman, M.M. Wintrobe, W. Dameshek, M.J. Goodman, A. Gilman, M. T. Mclennan, Nitrogen mustard therapy: use of methyl-bis(beta-chloroethyl)amine hydrochloride and tris(Beta-Chloroethyl)amine hydrochloride for hodgkin's disease, lymphosarcoma, leukemia and certain allied and miscellaneous disorders, J. Am. Med. Assoc. 132 (1946) 126–132.
[7] R.W. Shafer, D.A. Vuitton, Highly active antiretroviral therapy (HAART) for the treatment of infection with human immunodeficiency virus type 1, Biomed. Pharmacother. 53 (1999) 73–86.
[8] P.Y. Teo, W. Cheng, J.L. Hedrick, Y.Y. Yang, Co-delivery of drugs and plasmid DNA for cancer therapy, Adv. Drug Deliv. Rev. 98 (2016) 41–63.
[9] O. Pich, A. Cortes-Bullich, F. Muinos, M. Pratcorona, A. Gonzalez-Perez, N. Lopez-Bigas, The evolution of hematopoietic cells under cancer therapy, Nat. Commun. 12 (2021) 4803.
[10] H.K. Zhao, L. Wu, G.F. Yan, Y. Chen, M.Y. Zhou, Y.Z. Wu, Y.S. Li, Inflammation and tumor progression: signaling pathways and targeted intervention, Signal Transduct. Tar. 6 (2021) 263.
[11] I. Martinez-Reyes, N.S. Chandel, Mitochondrial TCA cycle metabolites control physiology and disease, Nat. Commun. 11 (2020) 102.
[12] D. Guo, Y. Tong, X. Jiang, Y. Meng, H. Jiang, L. Du, Q. Wu, S. Li, S. Luo, M. Li, L. Xiao, H. He, X. He, Q. Yu, J. Fang, Z. Lu, Aerobic glycolysis promotes tumor immune evasion by hexokinase2-mediated phosphorylation of IκBα, Cell Metabol. 34 (2022) 1312–1324.e6.
[13] N. Qin, L. Li, X. Ji, R. Pereira, Y. Chen, S. Yin, C. Li, X. Wan, D. Qiu, J. Jiang, H. Luo, Y. Zhang, G. Dong, Y. Zhang, S. Shi, H.J. Jessen, J. Xia, Y. Chen, C. Larsson, T. Tan, Z. Liu, J. Nielsen, Flux regulation through glycolysis and respiration is balanced by inositol pyrophosphates in yeast, Cell 186 (2023) 748–763.e715.
[14] X.J. Zhang, F. Luo, S.L. Luo, L. Li, X.X. Ren, J. Lin, Y.C. Liang, C. Ma, L.H. Ding, D. Y. Zhang, T.X. Ye, Y.N. Lin, B.L. Jin, S. Gao, Q.N. Ye, Transcriptional repression of aerobic glycolysis by OVOL2 in breast cancer, Adv. Sci. 9 (2022) 2200705.
[15] M.V. Liberti, J.W. Locasale, The Warburg effect: how does it benefit cancer cells? Trends Biochem. Sci. 41 (2016) 287, 287.
[16] I. Martinez-Reyes, N.S. Chandel, Cancer metabolism: looking forward, Nat. Rev. Cancer 21 (2021) 669–680.
[17] R. Zappasodi, I. Serganova, I.J. Cohen, M. Maeda, M. Shindo, Y. Senbabaoglu, M. J. Watson, A. Leftin, R. Maniyar, S. Verma, M. Lubin, M. Ko, M.M. Mane, H. Zhong, C. Liu, A. Ghosh, M. Abu-Akeel, E. Ackerstaff, J.A. Koutcher, P.C. Ho, G. M. Delgoffe, R. Blasberg, J.D. Wolchok, T. Merghoub, CTLA-4 blockade drives loss of T(reg) stability in glycolysis-low tumours, Nature 591 (2021) 652–658.
[18] S. Delaunay, G. Pascual, B.H. Feng, K. Klann, M. Behm, A. Hotz-Wagenblatt, K. Richter, K. Zaoui, E. Herpel, C. Munch, S. Dietmann, J. Hess, S.A. Benitah, M. Frye, Mitochondrial RNA modifications shape metabolic plasticity in metastasis, Nature 607 (2022) 593–603.
[19] S. Maschalidi, P. Mehrotra, B.N. Keçeli, H.K.L. De Cleene, K. Lecomte, R. Van der Cruyssen, P. Janssen, J. Pinney, G. van Loo, D. Elewaut, A. Massie, E. Hoste, K. S. Ravichandran, Targeting SLC7A11 improves efferocytosis by dendritic cells and wound healing in diabetes, Nature 608 (2022) E29. E29.
[20] N.A. Jiang, B.W. Xie, W.W. Xiao, M. Fan, S.X. Xu, Y.X. Duan, Y. Hamsafar, A. C. Evans, J. Huang, W.B. Zhou, X.L. Lin, N.R. Ye, S. Wanggou, W. Chen, D. Jing, R. C. Fragoso, B.N. Dugger, P.F. Wilson, M.A. Coleman, S.L. Xia, X.J. Li, L.Q. Sun, A. M. Monjazeb, A.J. Wang, W.J. Murphy, H.J. Kung, K.S. Lam, H.W. Chen, J.J. Li, Fatty acid oxidation fuels glioblastoma radioresistance with CD47-mediated immune evasion, Nat. Commun. 13 (2022) 1511.
[21] S. Kumagai, S. Koyama, K. Itahashi, T. Tanegashima, Y. Lin, Y. Togashi, T. Kamada, T. Irie, G. Okumura, H. Kono, D. Ito, R. Fujii, S. Watanabe, A. Sai, S. Fukuoka, E. Sugiyama, G. Watanabe, T. Owari, H. Nishinakamura, D. Sugiyama, Y. Maeda, A. Kawazoe, H. Yukami, K. Chida, Y. Ohara, T. Yoshida, Y. Shinno, Y. Takeyasu, M. Shirasawa, K. Nakama, K. Aokage, J. Suzuki, G. Ishii, T. Kuwata, N. Sakamoto, M. Kawazu, T. Ueno, T. Mori, N. Yamazaki, M. Tsuboi, Y. Yatabe, T. Kinoshita, T. Doi, K. Shitara, H. Mano, H. Nishikawa, Lactic acid promotes PD-1 expression in regulatory T cells in highly glycolytic tumor microenvironments, Cancer Cell 40 (2022) 201–218.e9.
[22] Z.E. Stine, Z.T. Schug, J.M. Salvino, C.V. Dang, Targeting cancer metabolism in the era of precision oncology, Nat. Rev. Drug Discov. 21 (2022) 141–162.
[23] F.S. Li, J.K. Weng, Demystifying traditional herbal medicine with modern approaches, Nat. Plants 3 (2017) 17109.
[24] A. Cravens, J. Payne, C.D. Smolke, Synthetic biology strategies for microbial biosynthesis of plant natural products, Nat. Commun. 10 (2019) 2142.
[25] H. Zubair, M.A. Khan, S. Anand, S.K. Srivastava, S. Singh, A.P. Singh, Modulation of the tumor microenvironment by natural agents: implications for cancer prevention and therapy, Semin. Cancer Biol. 80 (2022) 237–255.
[26] X.M. Xi, J.T. Wang, Y. Qin, W.D. Huang, Y.L. You, J.C. Zhan, Glycosylated modification of MUC1 maybe a new target to promote drug sensitivity and efficacy for breast cancer chemotherapy, Cell Death Dis. 13 (2022) 708.
[27] J. Heo, J. Lee, Y.J. Nam, Y. Kim, H. Yun, S. Lee, H. Ju, C.M. Ryu, S.M. Jeong, J. Lee, J. Lim, Y.M. Cho, E.M. Jeong, B. Hong, J. Son, D.M. Shin, The CDK1/TFCP2L1/ID2 cascade offers a novel combination therapy strategy in a preclinical model of bladder cancer, Exp. Mol. Med. 54 (2022) 801–811.
[28] Y.W. Li, J. Xu, G.Y. Zhu, Z.J. Huang, Y. Lu, X.Q. Li, N. Wang, F.X. Zhang, Apigenin suppresses the stem cell-like properties of triple-negative breast cancer cells by inhibiting YAP/TAZ activity, Cell Death Dis. 4 (2018) 105.
[29] Z.B. Jiang, W.J. Wang, C. Xu, Y.J. Xie, X.R. Wang, Y.Z. Zhang, J.M. Huang, M. Huang, C. Xie, P. Liu, X.X. Fan, Y.P. Ma, P.Y. Yan, L. Liu, X.J. Yao, Q.B. Wu, E.L. H. Leung, Luteolin and its derivative apigenin suppress the inducible PD-L1 expression to improve anti-tumor immunity in KRAS-mutant lung cancer, Cancer Lett. 515 (2021) 36–48.
[30] A.A. Mahbub, C.L. Le Maitre, N.A. Cross, N. Jordan-Mahy, The effect of apigenin and chemotherapy combination treatments on apoptosis-related genes and proteins in acute leukaemia cell lines, Sci. Rep. 12 (2022) 8858.
[31] Y. Songyang, W. Li, W.Q. Li, J. Yang, T.B. Song, The inhibition of GLUT1-induced glycolysis in macrophage by phloretin participates in the protection during acute lung injury, Int. Immunopharm. 110 (2022) 109049.
[32] R. Liu, Q. Liang, J.Q. Luo, Y.X. Li, X. Zhang, K.L. Fan, J.Z. Du, Ferritin-based nanocomposite hydrogel promotes tumor penetration and enhances cancer chemoimmunotherapy, Adv. Sci. 11 (2024) e2305217.
[33] Z.D. Dai, Q.H. Zhang, X.H. Li, Q. Chen, J.F. Chen, M. Wang, H.R. Chen, In situ forming pH/ROS-responsive niche-like hydrogel for ultrasound-mediated multiple therapy in synergy with potentiating anti-tumor immunity, Mater. Today 65 (2023) 62–77.
[34] C. Wang, J.Q. Wang, X.D. Zhang, S.J. Yu, D. Wen, Q.Y. Hu, Y.Q. Ye, H. Bomba, X. L. Hu, Z. Liu, G. Dotti, Z. Gu, In situ formed reactive oxygen species-responsive scaffold with gemcitabine and checkpoint inhibitor for combination therapy, Sci. Transl. Med. 10 (2018) eaan3682.
[35] L.Q. Wang, Z.H. Xu, H. Zhang, C.P. Yao, A review on chitosan-based biomaterial as carrier in tissue engineering and medical applications, Eur. Polym. J. 191 (2023) 112059.
[36] T. Kean, M. Thanou, Biodegradation, biodistribution and toxicity of chitosan, Adv. Drug Deliv. Rev. 62 (2010) 3–11.
[37] H.T. Ruan, Q.Y. Hu, D. Wen, Q. Chen, G.J. Chen, Y.F. Lu, J.Q. Wang, H. Cheng, W. Y. Lu, Z. Gu, A dual-bioresponsive drug-delivery depot for combination of epigenetic modulation and immune checkpoint blockade, Adv. Mater. 31 (2019) e1806957.
[38] D.M. Zhu, H. Chen, C.Y. Huang, G.X. Li, X. Wang, W. Jiang, K.L. Fan, H_2O_2 self-producing single-atom nanozyme hydrogels as light-controlled oxidative stress amplifier for enhanced synergistic therapy by transforming "cold" tumors, Adv. Funct. Mater. 32 (2022) 2110268.
[39] J. Kim, D.M. Francis, L.F. Sestito, P.A. Archer, M.P. Manspeaker, M.J. O'Melia, S. N. Thomas, Thermosensitive hydrogel releasing nitric oxide donor and anti-CTLA-4 micelles for anti-tumor immunotherapy, Nat. Commun. 13 (2022) 1479.
[40] Z.M. Li, W.G. Xu, J.Z. Yang, J. Wang, J.L. Wang, G. Zhu, D. Li, J.X. Ding, T.M. Sun, A tumor microenvironments-adapted polypeptide hydrogel/nanogel composite boosts antitumor molecularly targeted inhibition and immunoactivation, Adv. Mater. 34 (2022) e2200449.
[41] S. Huang, X. Kong, Y.S. Xiong, X.R. Zhang, H. Chen, W.Q. Jiang, Y.Z. Niu, W.L. Xu, C.G. Ren, An overview of dynamic covalent bonds in polymer material and their applications, Eur. Polym. J. 141 (2020) 110094.
[42] S.B. Manjare, R.K. Mahadik, K.S. Manval, P.P. More, S.S. Dalvi, Microwave-assisted rapid and green synthesis of Schiff bases using cashew shell extract as a natural acid catalyst, ACS Omega 8 (2023) 473–479.
[43] J.L. Yang, C.C. Pi, G.H. Wang, Inhibition of PI3K/Akt/mTOR pathway by apigenin induces apoptosis and autophagy in hepatocellular carcinoma cells, Biomed. Pharmacother. 103 (2018) 699–707.
[44] M.A. Tempero, U. Pelzer, E.M. O'Reilly, J. Winter, D. Oh, C.P. Li, G. Tortora, H. M. Chang, C.D. Lopez, T. Bekaii-Saab, A.H. Ko, A. Santoro, J.O. Park, M.S. Noel, G. L. Frassineti, Y.S. Shan, A. Dean, H. Riess, E. Van Cutsem, J. Berlin, P. Philip, M. Moore, D. Goldstein, J. Tabernero, M.Y. Li, S. Ferrara, Y. Le Bruchec, G. Zhang, B. Lu, A.V. Biankin, M. Reni, A. Investigators, Adjuvant *nab*-paclitaxel + gemcitabine in resected pancreatic ductal adenocarcinoma: results from a randomized, open-label, phase III trial, J. Clin. Oncol. 41 (2023) 2007–2019.